

Climate sensitivity from both physical and carbon cycle feedbacks

Philip Goodwin¹, Richard G. Williams², Vassil Roussenov² and Anna Katavouta²

Re-submission to GRL

6th June 2019

¹Ocean and Earth Science, National Oceanography Centre Southampton, University of Southampton, Southampton, UK

²Department of Earth, Ocean & Ecological Sciences, School of Environmental Sciences, University of Liverpool, Liverpool, UK.

ORCID ID P. Goodwin: 0000-0002-2575-8948

ORCID ID R.G. Williams: 0000-0002-3180-7558

ORCID ID V. Roussenov: 0000-0003-4128-9712

ORCID ID A. Katavouta: 0000-0002-1587-4996

Abstract

The surface warming response to anthropogenic forcing is highly sensitive to the strength of feedbacks in both the physical climate and carbon-cycle systems. However, the definitions of climate feedback, λ_{Climate} in $\text{Wm}^{-2}\text{K}^{-1}$, and climate sensitivity, S_{Climate} in $\text{K}[\text{Wm}^{-2}]^{-1}$, explicitly exclude the impact of carbon-cycle feedbacks. Here, we provide a new framework to incorporate carbon feedback into the definitions of climate feedback and sensitivity. Applying our framework to the Global Carbon Budget reconstructions reveals a present-day terrestrial carbon feedback of $\lambda_{\text{Carbon}}=0.31\pm 0.09 \text{ Wm}^{-2}\text{K}^{-1}$ and an ocean carbon feedback of -0.06 to $0.015 \text{ Wm}^{-2}\text{K}^{-1}$ in Earth system models. Observational constraints reveal a combined climate and carbon feedback of $\lambda_{\text{Climate+Carbon}}=1.48 \text{ Wm}^{-2}\text{K}^{-1}$ with a 95% range of 0.76 to $2.32 \text{ Wm}^{-2}\text{K}^{-1}$ on centennial timescales, corresponding to a combined climate and carbon sensitivity of $S_{\text{Climate+Carbon}}=0.67 \text{ K}[\text{Wm}^{-2}]^{-1}$ with a 95% range of 0.43 to $1.32 \text{ K}[\text{Wm}^{-2}]^{-1}$.

Plain Language Summary

35
36
37
38
39
40
41
42
43
44
45
46
47
48
49
50
51
52
53

Feedback processes in the physical climate system and the carbon cycle affect the Earth's climate response to emissions of greenhouse gases, such as carbon dioxide. Physical climate feedbacks include the responses of clouds and atmospheric water vapor to rising surface temperatures, while carbon cycle feedbacks affect how much of the emitted carbon dioxide is removed from the atmosphere and stored in the ocean and on land. Conventionally, definitions of climate feedback and climate sensitivity include all the feedbacks in the physical climate system, but do not include carbon cycle feedbacks. This study provides a new framework to incorporate carbon feedback into the definitions of climate feedback and sensitivity. Evaluating the historical strengths of physical climate system and carbon cycle feedbacks suggests emissions of carbon dioxide will cause equilibrium (century timescale) surface warming to increase by between 0.6 to 2.0 °C for every 1000 PgC emitted when an equilibrium is approached between the atmosphere and ocean over many centuries.

54 **1. Introduction**

55 Climate change is driven by a combination of radiative forcing and climate feedbacks operating in
56 the climate system (see review in *Knutti et al.*, 2017). The climate feedback is usually expressed in
57 terms of the change in surface temperature multiplied by a feedback parameter, λ in $\text{Wm}^{-2}\text{K}^{-1}$,
58 defined in terms of a wide range of physical processes, including the Planck response of enhanced
59 longwave emission from a warmer surface and physical feedbacks from changes in water vapour,
60 lapse rate, cloud cover and ice albedo (*Gregory et al.*, 2004; *Andrews et al.*, 2012, *Armour et al.*,
61 2013; *Andrews et al.*, 2015; *Ceppi and Gregory*, 2017). In contrast, the carbon-cycle responses and
62 feedbacks are usually defined in terms of how atmospheric carbon dioxide and temperature linearly
63 combine to alter the carbon inventories of the climate system (*Friedlingstein et al.*, 2003, 2006;
64 *Arora et al.*, 2013), which may be expressed in terms of a radiative feedback parameter in $\text{Wm}^{-2}\text{K}^{-1}$
65 (*Gregory et al.*, 2009). However, there are difficulties in applying this carbon feedback method due
66 to nonlinearities in how the separate atmospheric carbon dioxide and temperature effects combine
67 together (*Schwinger et al.*, 2014) giving rise to errors in the overall carbon feedback (*Arora et al.*,
68 2013). This linearization method also cannot be used to calculate the carbon feedback directly from
69 observational reconstructions of the carbon cycle (e.g. *le Quéré et al.*, 2018), since there is no
70 observational method to generate the hypothetical state with a range of feedback processes turned
71 off for the real world.

72
73 The separation of forcing and feedback is dependent upon the nature of the climate perturbation. In
74 climate model experiments driven by an imposed atmospheric CO_2 trajectory, a radiative forcing is
75 provided from the increase in atmospheric CO_2 that automatically includes the effects of carbon-
76 cycle feedbacks. In contrast, for climate model experiments driven by carbon emissions, a radiative
77 forcing is provided from the increase in atmospheric CO_2 directly caused by the carbon emission
78 together with a radiative feedback from the change in atmospheric CO_2 caused by changes in the
79 terrestrial and ocean carbon reservoirs.

80
81 To understand this distinction between forcing and feedback, consider the response of a conceptual
82 Earth system model to a pulse of carbon released to the atmosphere, which is partitioned between
83 the atmosphere, ocean and terrestrial systems (Fig. 1a). The original carbon release drives a
84 radiative forcing from the increase in atmospheric CO_2 (Fig. 1b, red line), which is augmented by a
85 radiative feedback from both non- CO_2 and CO_2 changes (Fig. 1c, yellow and blue lines). These
86 feedbacks may act to enhance or oppose the original forcing perturbation.

87

88 Our aim is to define and evaluate a new feedback parameter for the carbon system that:
 89 (1) Takes into account the combined effects of the non-CO₂ and CO₂ feedbacks operating in the
 90 climate system, thus avoiding the need to make a linearizing assumption that introduces error;
 91 (2) Allows direct comparison between magnitudes of, and uncertainties in, feedbacks in the climate
 92 and carbon systems; and
 93 (3) Allows the practical application of real-world observational data to analyze carbon feedback.

94

95 **2. Definition of a climate and carbon feedback parameter**

96 Consider the global energy balance for a climate system perturbed from an initial steady state (e.g.
 97 Fig. 1a,b). The radiative forcing perturbation, $\Delta R'$, from the original forcing perturbation combined
 98 with subsequent feedback terms is balanced by additional outgoing longwave radiation emitted due
 99 to surface warming, $\lambda_{Planck}\Delta T$, and the net Earth system heat uptake, N , all terms defined in Wm^{-2} ,
 100

$$101 \quad \Delta R' = \lambda_{Planck}\Delta T + N, \quad (1)$$

102

103 where λ_{Planck} is the Planck feedback parameter in $\text{Wm}^{-2}\text{K}^{-1}$ and ΔT is the change in global-mean
 104 surface temperature in K. The radiative forcing, $\Delta R'$, consists of an original forcing perturbation,
 105 $\Delta R^{forcing}$ plus a subsequent feedback term, $\Delta R^{feedback}$, $\Delta R' = \Delta R^{forcing} + \Delta R^{feedback}$, and the
 106 feedback may be written in terms of the separate non-CO₂ and CO₂ components, $\Delta R_{non-CO_2}^{feedback}$ and
 107 $\Delta R_{CO_2}^{feedback}$ respectively (Fig. 1b), such that

108

$$109 \quad \Delta R' = \Delta R^{forcing} + \Delta R_{non-CO_2}^{feedback} + \Delta R_{CO_2}^{feedback}. \quad (2)$$

110

111 The radiative feedback term from non-CO₂ feedbacks, $\Delta R_{non-CO_2}^{feedback}$, includes the effects of changes
 112 in water vapor, lapse rate, clouds and surface albedo, while the radiative feedback term from CO₂,
 113 $\Delta R_{CO_2}^{feedback}$, includes how radiative forcing from atmospheric CO₂ is altered by changes in the
 114 ocean and terrestrial carbon inventories.

115

116 The radiative response is often defined in terms of a climate feedback, $\lambda_{Climate}\Delta T$ in Wm^{-2} , by
 117 combining the Planck response, $\lambda_{Planck}\Delta T$, with the radiative forcing from non-CO₂ feedbacks,
 118 $\Delta R_{non-CO_2}^{feedback}$ (e.g. see IPCC, 2013; Knutti *et al.*, 2017),

119

$$120 \quad \lambda_{Climate}\Delta T = \lambda_{Planck}\Delta T - \Delta R_{non-CO_2}^{feedback}, \quad (3)$$

121

122 such that the energy balance in (1) may be re-expressed from (2) and (3) by

123

$$124 \quad \Delta R^{forcing} + \Delta R_{CO_2}^{feedback} = \lambda_{Planck} \Delta T - \Delta R_{non-CO_2}^{feedback} + N = \lambda_{Climate} \Delta T + N. \quad (4)$$

125

126 The standard form of the climate feedback definition in (3) does not encapsulate the full sensitivity
 127 of the Earth system to perturbation, as the definition only accounts for the strength of the non-CO₂
 128 feedbacks in the system and ignores the impact of carbon-cycle feedbacks, which are instead treated
 129 as part of the forcing perturbation in (4). Here, we re-express the energy-balance relations (1) and
 130 (4) using a new combined carbon plus climate feedback, $\lambda_{Climate+Carbon}$ in $Wm^{-2}K^{-1}$, defined as the
 131 sum of the climate and carbon feedbacks,

132

$$133 \quad \lambda_{Climate+Carbon} \Delta T = \lambda_{Planck} \Delta T - \Delta R_{non-CO_2}^{feedback} - \Delta R_{CO_2}^{feedback} = (\lambda_{Climate} + \lambda_{Carbon}) \Delta T,$$

134 (5)

135

136 where $\lambda_{Carbon} = -\Delta R_{CO_2}^{feedback} / \Delta T$. The energy balance in (1) may now be more explicitly written
 137 in terms of the original radiative forcing, $\Delta R^{forcing}$, balancing the radiative response from the
 138 combined climate and carbon responses, $\lambda_{Climate+Carbon} \Delta T$, plus the planetary heat uptake, N ,
 139 such that

140

$$141 \quad \Delta R^{forcing} = \lambda_{Climate} \Delta T - \Delta R_{CO_2}^{feedback} + N = \lambda_{Climate+Carbon} \Delta T + N. \quad (6)$$

142

143 To progress, we now wish to evaluate the carbon feedback λ_{Carbon} in terms of changes in ocean
 144 and terrestrial carbon inventories.

145

146 **3. Extracting the feedback component to CO₂ change**

147 A small carbon emission into a preindustrial state, δI_{em} in PgC, is distributed between the
 148 atmospheric, ocean and terrestrial carbon reservoirs (Fig. 1a),

149

$$150 \quad \delta I_{em} = \delta I_{atmos} + \delta I_{ocean} + \delta I_{ter} = M \delta CO_2 + V \delta C_{DIC} + \delta I_{ter}, \quad (7)$$

151

152 where $\delta I_{atmos} = M \delta CO_2$ is the change in atmospheric CO₂ inventory since the preindustrial, with M
 153 the molar volume of the atmosphere and CO₂ the atmospheric CO₂ mixing ratio; $\delta I_{ocean} = V \delta C_{DIC}$ is

154 the change in ocean dissolved inorganic carbon (DIC) inventory, with V the ocean volume and C_{DIC}
 155 the mean-ocean concentration of DIC; δI_{ter} is the change in terrestrial (soil + vegetation) carbon
 156 inventory; and the symbol δ is used to indicate a small infinitesimal change since the preindustrial.
 157

158 Radiative forcing is related to the log change in atmospheric CO_2 , $R_{\text{CO}_2} = a\Delta \ln \text{CO}_2$ (Myhre *et al.*,
 159 2013), so that our goal is to find an expression for the change in log CO_2 due to some initial carbon
 160 emission, δI_{em} , and subsequent responses to forcing and feedbacks within the atmosphere-ocean-
 161 terrestrial carbon system (7). The ocean inventory of carbon involves the dissolved inorganic
 162 carbon concentration C_{DIC} , which may be expressed as a sum of process-driven components (Ito
 163 and Follows, 2005; Goodwin *et al.*, 2008, Williams and Follows, 2011) involving the DIC
 164 concentration at chemical saturation with atmospheric CO_2 , C_{sat} , the disequilibrium concentration at
 165 subduction, C_{dis} , and the DIC contribution from regenerated biological material, C_{bio} ,
 166 ($C_{DIC} = C_{sat} + C_{dis} + C_{bio}$: Appendix). Applying this ocean partitioning allows the perturbation to the
 167 global carbon inventory (7) to be re-expressed as
 168

$$\delta I_{em} = \left(I_{atmos} + \frac{VC_{sat}}{B} \right) \delta \ln \text{CO}_2 + V \left(\delta C_{dis} + \delta C_{bio} + \frac{\partial C_{sat}}{\partial A_{pre}} \delta A_{pre} + \frac{\partial C_{sat}}{\partial T_{oc}} \delta T_{oc} \right) + \delta I_{ter}, \quad (8)$$

169
 170
 171 where A_{pre} is the global mean ocean preformed titration alkalinity; T_{oc} is the global mean ocean
 172 temperature; $B = \partial \ln \text{CO}_2 / \partial \ln C_{sat}$ is the Revelle Buffer factor of seawater; and $I_{atmos} +$
 173 $(VC_{sat}/B) = I_B$ is the buffered carbon inventory of the air-sea system (Goodwin *et al.*, 2007;
 174 2008; 2015).
 175

176 Re-arranging (8) for $\delta \ln \text{CO}_2$, and integrating for large changes using a constant buffered carbon
 177 inventory approximation (Goodwin *et al.*, 2007; 2008; 2009; 2011; 2015: Appendix), decomposes
 178 ΔR_{CO_2} into the initial response to forcing from anthropogenic carbon emissions in the absence of
 179 feedbacks, $\Delta R_{\text{CO}_2}^{forcing}$, plus components from terrestrial and ocean carbon cycle feedbacks,

180 $\Delta R_{\text{CO}_2}^{feedback} = \Delta R_{\text{CO}_2}^{feedback_{terrestrial}} + \Delta R_{\text{CO}_2}^{feedback_{ocean}}$ (Fig. 1a,b), such that

$$\Delta R_{\text{CO}_2} = \Delta R_{\text{CO}_2}^{forcing} + \Delta R_{\text{CO}_2}^{feedback} = \Delta R_{\text{CO}_2}^{forcing} + \Delta R_{\text{CO}_2}^{feedback_{terrestrial}} + \Delta R_{\text{CO}_2}^{feedback_{ocean}}, \quad (9)$$

183

184 where $\Delta R_{CO_2}^{forcing}$ is related to terms involving the carbon emission ΔI_{em} and the change in ocean
 185 disequilibrium carbon ΔC_{dis} from (8); $\Delta R_{terrestrial}^{feedback}$ is related to the feedback from the change in the
 186 terrestrial carbon inventory, ΔI_{ter} ; and $\Delta R_{ocean}^{feedback}$ is related to the feedback from the changes in the
 187 ocean carbon inventory involving the saturated and regenerated carbon pools (8) from ΔC_{bio} , ΔA_{pre}
 188 and ΔT_{oc} (Appendix).

189

190 **4. Evaluating carbon feedback from observational constraints and numerical simulations**

191

192 **4.1 Terrestrial carbon feedback**

193 The change in the radiative forcing, $\Delta R_{terrestrial}^{feedback}$ in (9), is related to the change in the cumulative
 194 terrestrial carbon inventory relative to the preindustrial, ΔI_{ter} in PgC (Fig. 1a,b; *Goodwin et al.*,
 195 2007; 2008; 2009; 2011; 2015: Appendix), which is given by

196

$$197 \quad \Delta R_{terrestrial}^{feedback} = -\left(\frac{a}{I_B}\right) \Delta I_{ter}. \quad (10)$$

198

199 The terrestrial carbon feedback λ_{Carbon} is diagnosed from reconstructions of the change in the
 200 terrestrial carbon inventory and surface temperature record by substituting (10) into (5),

201

$$202 \quad \lambda_{Carbon} = -\frac{\Delta R_{terrestrial}^{feedback}}{\Delta T} = -\left(\frac{a}{I_B}\right) \frac{\Delta I_{ter}}{\Delta T} \quad (11)$$

203 This new relation (11) is now used to quantify terrestrial carbon feedback from observational
 204 reconstructions and Earth system model simulations. λ_{Carbon} is estimated using the following
 205 parameters: the radiative forcing coefficient from CO₂, $a=5.35\pm 0.27$ Wm⁻² (*Myhre et al.*, 2013); the
 206 buffered carbon inventory, $I_B=3451\pm 96$ PgC (*Williams et al.*, 2017); the global-mean surface
 207 temperature change ΔT is from the GISTEMP temperature record (*Hansen et al.* 2010), including
 208 an 11-average smoothing (Fig. 2a, black dotted and full lines); and change in the terrestrial carbon
 209 inventory ΔI_{ter} are from the Global Carbon Budget (*le Quéré et al.*, 2018) (Fig. 2b, black).

210 Uncertainties in the terrestrial carbon budget are taken from the additional data for the 16 individual
 211 dynamic global vegetation models (DGVMs) in the Global Carbon Budget (*le Quéré et al.*, 2018;
 212 Supplementary Information; Acknowledgements).

213

214 These historical reconstructions for the terrestrial carbon inventory and surface temperature reveal
215 an observation-constrained estimate of the terrestrial carbon feedback parameter, $\lambda_{\text{Carbon}}=0.33\pm 0.09$
216 $\text{Wm}^{-2}\text{K}^{-1}$ for the present day (Fig. 2c, black line and shading), which represents a negative feedback
217 that reduces global warming through terrestrial carbon uptake. The strength of this negative
218 feedback reached a peak magnitude of $\lambda_{\text{Carbon}}=0.86\pm 0.34 \text{ Wm}^{-2}\text{K}^{-1}$ in the late 1960s, but then has
219 decreased in time as the rate of increase in surface warming since the early 1970s (Fig. 2a, black)
220 (*Hansen et al.*, 2010) has not matched the rate of increase in the cumulative terrestrial carbon sink
221 (Fig. 2b, black) (*le Quéré et al.*, 2018).

222

223 The terrestrial carbon feedback is now evaluated from four CMIP5 Earth system models
224 (CanESM2, HadGEM2-ES, HadGEM2-CC and NorESM-ME), chosen as these have a reliable net
225 export production (nep) variable allowing calculation of ΔI_{ter} in (11). From the simulated ΔI_{ter} and
226 11-year average ΔT (Fig. 2a,b), and estimates of a and I_B for each model (*Williams et al.* 2017),
227 λ_{Carbon} is evaluated from year 1959 to 2100 for the RCP4.5 scenario (Fig. 2c). These four CMIP5
228 Earth system models have a smaller present-day terrestrial carbon feedback parameter ranging from
229 0.02 to $0.65 \text{ Wm}^{-2}\text{K}^{-1}$, broader than the 1σ range from observational reconstructions (Fig. 2c,
230 compare dashed lines to black line and shading). These differences between the Earth system
231 models and the observational estimate arise from their discrepancy between the modeled and
232 observational reconstructions of surface warming and terrestrial carbon uptake (Fig. 2a,b). The
233 future simulated λ_{Carbon} remains stable under the RCP4.5 scenario, remaining close to the present-
234 day values to year 2100 (Fig 2c).

235

236 Additional projections of carbon feedback are made using a very large ensemble of observation-
237 constrained simulations from the Warming Acidification and Sea level Projector (WASP: *Goodwin*,
238 2016), for the RCP4.5 scenario (Fig. 2, blue line and shading). We adopt the WASP model
239 configuration of *Goodwin* (2018), with climate feedback including components from different
240 processes operating on different response timescales (Fig. 1). An ensemble is generated of many
241 thousands of observation-consistent simulations using the Monte Carlo plus history matching
242 (*Williamson et al.*, 2015) methodology of *Goodwin et al.* (2018). First, the initial ensemble of 10-
243 million Monte Carlo simulations is generated as in *Goodwin* (2018), with varied model input
244 parameters, and integrate each simulation from years 1765 to 2017 with historical forcing. Next the
245 observational-consistency test of *Goodwin* (2018 – see Table 2 therein) is applied with an updated
246 terrestrial carbon range (Supplementary Table S1) based on the 16 observation-consistent DGVMs
247 of the Global Carbon Budget 2018 (*le Quéré et al.* 2018). Only 6273 simulations pass the

248 observation-consistency test and a further 3 simulations are rejected as non-physical since λ_{Climate}
 249 becomes negative on long timescales.

250

251 The remaining ensemble of 6270 WASP simulations are then consistent with historic observations
 252 of surface warming (Fig. 2a, compare blue to black), terrestrial carbon uptake (Fig. 2b, compare
 253 blue to black) and ocean heat content changes (Supplementary Table S1; Goodwin, 2018). Due to
 254 the observation-simulation agreement in ΔT and ΔI_{ter} , the final WASP ensemble is also in good
 255 agreement with the observational reconstructions of terrestrial λ_{Carbon} using (11) from years 1959 to
 256 2017 (Fig. 2c, compare blue to black). Under the RCP4.5 scenario, the observation-constrained
 257 WASP ensemble shows a similar future behavior as in the response of the CMIP5 models (Fig. 2c,
 258 compare blue solid line and shading to dashed lines), with λ_{Carbon} displaying only a small change in
 259 magnitude from the present day towards year 2100.

260

261 4.2 Ocean carbon feedback

262 In a similar manner to how the terrestrial carbon feedback is defined relative to ΔI_{ter} (11), the ocean
 263 carbon feedback is defined in relation to changes in the ocean DIC from regenerated carbon, ΔC_{bio} ,
 264 and changes in the ocean saturated carbon inventory from preformed alkalinity ΔA_{pre} and ocean
 265 temperature ΔT_{oc} (eqns. 8, A8), via,

266

$$\lambda_{\text{Carbon}} = -\frac{\Delta R_{\text{ocean}}^{\text{feedback}}}{\Delta T} = -\left(\frac{\alpha}{I_B}\right) \frac{\Delta C_{\text{bio}} + (\partial C_{\text{sat}}/\partial A_{\text{pre}})\Delta A_{\text{pre}} + (\partial C_{\text{sat}}/\partial T_{\text{oc}})\Delta T_{\text{oc}}}{\Delta T}.$$

(12)

267

268 This ocean feedback term represents how changes in ocean temperature and ocean biological
 269 cycling of carbon and alkalinity from an initial carbon perturbation then feedback to alter the
 270 radiative forcing from atmospheric CO₂. Based on Earth system models (evaluating ΔC_{bio} , ΔA_{pre}
 271 and ΔT_{oc}), observational reconstructions for ocean heat uptake (*Cheng et al.*, 2017) and the WASP
 272 ensemble (both evaluating ΔT_{oc} only), the ocean carbon feedback is diagnosed as being much
 273 smaller than the terrestrial carbon feedback in the present day, ranging from -0.015 to 0.06 Wm⁻²K⁻¹
 274 (Fig. 2c,d), and remains small for the 21st century. The magnitude of the ocean carbon feedback
 275 might though increase beyond year 2100 due to continued climate-driven changes in ocean
 276 temperature, ΔT_{oc} , and ocean biological carbon drawdown, ΔC_{bio} .

277

278 Our estimate of ocean carbon feedback (Fig. 2d) is much smaller than that implied by *Gregory et al.*
 279 (2009) because the previous approach (*Friedlingstein et al.*, 2006) considers the transient

280 disequilibrium of ocean DIC, C_{dis} (eq. 8), to be part of the ocean carbon feedback, while our method
281 considers C_{dis} as part of the transient ocean response. An idealized feedback grows in magnitude
282 over time, from zero the instant a forcing is applied to some final equilibrium value on long
283 timescales. We do not consider C_{dis} part of the ocean carbon feedback because the time-evolution of
284 C_{dis} is the opposite sense: ocean CO₂ disequilibrium is large the instant CO₂ is emitted into the
285 atmosphere and then decays to zero over long timescales due to ocean carbon uptake
286 (Supplementary Fig. S1).

287

288 **5. Estimating the combined carbon-climate feedback and sensitivity**

289 We now place observational constraints on the combined climate plus carbon feedback,
290 $\lambda_{Climate+Carbon}$, and sensitivity, $S_{Climate+Carbon}$ in $K[Wm^{-2}]^{-1}$, by evaluating both $\lambda_{Climate}$ and λ_{Carbon} for an
291 idealized perturbation experiment in the observation constrained WASP ensemble. Each of the 6270
292 observation-consistent WASP ensemble members (Fig. 2, blue line and shading) is reinitialized at a
293 preindustrial spin up and integrated for 500 years, forced with an idealized scenario consisting of a
294 1000 PgC emission over the first 100 years (Fig. 1a).

295

296 The total radiative forcing R' is decomposed into the initial emission forcing, $\Delta R_{CO_2}^{forcing}$, non-CO₂
297 feedback, $\Delta R_{non-CO_2}^{feedback}$, and CO₂ feedback, $\Delta R_{CO_2}^{feedback}$, terms (Fig. 1b) using eqns. (1)-(6). From
298 this decomposition, $\lambda_{Climate}$ and λ_{Carbon} (Figs. 1c,d) are evaluated over multiple response timescales
299 in the observation-consistent ensemble, where the $\lambda_{Climate}$ results are comparable to the similarly
300 constrained ensemble in *Goodwin* (2018 – see figure 2 therein). Here, λ_{Carbon} in WASP includes
301 both the larger terrestrial and smaller ocean temperature-CO₂ solubility effects (Fig. 1d), but WASP
302 does not simulate changes in C_{bio} , which remain small in Earth system models (Fig. 2d). For
303 illustration purposes, $\lambda_{Climate}$ and λ_{Carbon} contributions from individual processes are shown by
304 integrating the WASP ensemble with combinations of feedback processes switched off (Fig. 1c,d,
305 dashed lines are ensemble median values).

306

307 Estimates of the carbon and climate feedback parameters, λ_{Carbon} and $\lambda_{Climate}$, applicable on century
308 timescales, are made from the observation-consistent ensemble distributions at the end of the
309 1000PgC emission simulations (Fig. 1). The 500-year carbon feedback after a 1000PgC emission
310 has a median (and 95% range) of $\lambda_{Carbon} = 0.21$ (-0.02 to 0.5) $Wm^{-2}K^{-1}$ (Fig. 1c), while the physical
311 climate feedback after a 1000PgC emission is $\lambda_{Climate} = 1.27$ (0.73 to 1.88) $Wm^{-2}K^{-1}$ (Fig. 1b, Fig 3a,
312 blue).

313

314 The impact of carbon feedbacks is therefore to increase the overall carbon plus climate feedback
315 above λ_{Climate} , with an observation-constrained distribution of $\lambda_{\text{Climate+Carbon}} = \lambda_{\text{Carbon}} + \lambda_{\text{Climate}} = 1.48$
316 (0.76 to 2.32) $\text{Wm}^{-2}\text{K}^{-1}$ (Fig. 3a). Consequently, the climate sensitivity, $S = 1/\lambda$, from non-CO₂
317 feedbacks alone, $S_{\text{Climate}} = 0.79$ (0.53 to 1.37) $\text{K}[\text{Wm}^{-2}]^{-1}$, is reduced to $S_{\text{Climate+Carbon}} = 0.67$ (0.43 to
318 1.32) $\text{K}[\text{Wm}^{-2}]^{-1}$, when encapsulating both non-CO₂ and CO₂ feedbacks acting together (Fig. 3b).
319 This estimate of $S_{\text{Climate+Carbon}}$ (Fig. 3b, black) represents the total sensitivity of the climate system to
320 perturbation by carbon emission over century timescales, including both physical climate and
321 carbon-cycle feedbacks.

322

323 6. Conclusions

324 A new method is presented to constrain the carbon feedback parameter, finding for the present-day
325 terrestrial carbon system $\lambda_{\text{Carbon}} = 0.33 \pm 0.09 \text{Wm}^{-2}\text{K}^{-1}$ (Fig. 2c) based on observational
326 reconstructions of carbon uptake and warming (*le Quéré et al. 2018; Hansen et al., 2010*), and
327 $\lambda_{\text{Carbon}} = 0.02$ to $0.65 \text{Wm}^{-2}\text{K}^{-1}$ in four CMIP5 models. This compares to a previous method implying
328 terrestrial carbon feedback of $\lambda_{\text{Carbon}} = 0.7 \pm 0.5 \text{Wm}^{-2}\text{K}^{-1}$, based on analysis of the earlier C4MIP
329 climate model ensemble (*Arneth et al., 2010; Gregory et al., 2009; Friedlingstein et al., 2006*) and
330 comprising a linearization of separate CO₂-carbon ($1.1 \pm 0.5 \text{Wm}^{-2}\text{K}^{-1}$) and climate-carbon
331 ($-0.4 \pm 0.2 \text{Wm}^{-2}\text{K}^{-1}$) components. The linearization assumed by the previous method introduces
332 errors (*Schwinger et al. 2014; Arora et al., 2013*) and means the method cannot be applied to
333 observational reconstructions. To avoid making the linearization assumption, and so be applicable
334 to observational reconstructions, our method assumes a constant buffered carbon inventory
335 (Appendix); a good approximation for carbon perturbations up to $\sim 5000 \text{PgC}$ or for atmospheric
336 CO₂ reaching $\sim 1100 \text{ppm}$ (*Goodwin et al., 2007; 2008; 2009*).

337

338 The Equilibrium Climate Response to Emission, ECRE in $\text{K } 1000 \text{PgC}^{-1}$, expresses the warming per
339 unit carbon emitted once ocean heat uptake approaches zero over centennial to multi-centennial
340 timescales, $\text{ECRE} = \Delta T / \Delta I_{em}$ (*Frölicher & Paynter 2015*). This atmosphere-ocean equilibrium is
341 approached over many centuries, but not necessarily reached due to the effect of other longer
342 timescale carbon and climate feedbacks, such as from ice sheet-albedo feedbacks (*Rohling et al.,*
343 *2018*) and multi-millennial CaCO₃ sediment and weathering responses (*Archer et al., 2005*). In the
344 absence of carbon feedbacks, *Williams et al. (2012)* related the ECRE to climate feedback, λ_{Climate} ,
345 via $\text{ECRE} = a / (\lambda_{\text{climate}} I_B)$. Here, we extend the relationship to include the effects of both climate
346 and carbon feedbacks, $\text{ECRE} = a / (\lambda_{\text{climate+carbon}} I_B)$, applicable after ocean CO₂ invasion and

347 heat uptake but prior to significant CaCO₃ sediment and weathering responses (Archer, 2005;
 348 Goodwin et al., 2007; 2008; 2015). Our historically constrained feedback estimates (Fig. 3a,b)
 349 imply ECRE=1.0 (0.6 to 2.0) K per 1000PgC emitted (Fig. 3c), with the upper half of our range
 350 (from 1 to 2 K[1000PgC]⁻¹) consistent with a CMIP5-based estimate (Frölicher & Paynter, 2015).
 351 Carbon and climate feedbacks not constrained historically (e.g. Rohling et al., 2018; Zickfield et al.,
 352 2013; Pugh et al., 2018; MacDougall & Knutti, 2016), may alter future $\lambda_{climate+carbon}$ and so alter
 353 ECRE. We anticipate this relationship, $ECRE = a/(\lambda_{climate+carbon}I_B)$, will be useful in elucidating
 354 how different carbon and climate feedbacks contribute to the multi-century warming response to
 355 carbon emission.

356

357 **Appendix: Connecting radiative feedbacks to changes in carbon inventories**

358

359 Our aim is to separate the total CO₂ radiative forcing into a sum of linearly-separable terms
 360 representing different processes and feedbacks. We start by considering how carbon emissions
 361 perturb carbon storage across the atmosphere-ocean-terrestrial system. We now write identities for
 362 the changes in atmospheric and ocean carbon inventories containing terms with $\delta \ln \text{CO}_2$. Using the
 363 identity for small perturbations in x , $\delta x = x \delta \ln x$, we write an identity for a small perturbation in
 364 atmospheric CO₂ inventory, δI_{atmos} , in terms of a small perturbation to the logarithm of atmospheric
 365 CO₂, $\delta \ln \text{CO}_2$,

366

$$367 \delta I_{atmos} = I_{atmos} \delta \ln \text{CO}_2, \quad (\text{A1})$$

368

369 where I_{atmos} is the initial atmospheric CO₂ inventory at the unperturbed preindustrial state.

370

371 The change in ocean DIC is considered, via a process-driven viewpoint (*Ito and Follows, 2005;*
 372 *Goodwin et al., 2008; Williams and Follows, 2011*), in terms of the sum of components from the
 373 change in chemically-saturated DIC arising from changes in atmospheric CO₂ and seawater
 374 properties, δC_{sat} , the change in chemical disequilibrium of ocean DIC relative to atmospheric CO₂,
 375 δC_{dis} , and the combined change in ocean DIC from regenerated soft tissue and CaCO₃ drawdown,
 376 δC_{bio} ,

377

$$378 \delta C_{DIC} = \delta C_{sat} + \delta C_{dis} + \delta C_{bio}. \quad (\text{A2})$$

379

380 Due to the carbonate chemistry system, the perturbation to C_{sat} is a function of the change to the
 381 logarithm of atmospheric CO_2 , $\delta \ln \text{CO}_2$, the change in mean ocean preformed titration alkalinity,
 382 δA_{pre} , the change in mean seawater temperature, δT_{oc} , and the change in mean seawater salinity, δS :

383 $C_{sat} = C_{sat}(\ln \text{CO}_2, A_{pre}, T_{oc}, S)$. This small perturbation to C_{sat} is now expanded after
 384 *Goodwin and Lenton (2009)* into components from $\delta \ln \text{CO}_2$, δA_{pre} , δT_{oc} , and δS ,

$$386 \quad \delta C_{dis} = \frac{\partial C_{sat}}{\partial \ln \text{CO}_2} \delta \ln \text{CO}_2 + \frac{\partial C_{sat}}{\partial A_{pre}} \delta A_{pre} + \frac{\partial C_{sat}}{\partial T_{oc}} \delta T_{oc} + \frac{\partial C_{sat}}{\partial S} \delta S, \quad (\text{A3})$$

387
 388 where the salinity term, $(\partial C_{sat}/\partial S)\delta S$, is small and henceforth will be omitted.

389
 390 Again, using the identity for small perturbations in a variable x , $\delta x = x \delta \ln x$, but applying to C_{sat} , the
 391 term for the sensitivity of C_{sat} to $\ln \text{CO}_2$ in (A3) becomes,

$$393 \quad \frac{\partial C_{sat}}{\partial \ln \text{CO}_2} \delta \ln \text{CO}_2 = C_{sat} \frac{\partial \ln C_{sat}}{\partial \ln \text{CO}_2} \delta \ln \text{CO}_2 = \frac{C_{sat}}{B} \delta \ln \text{CO}_2, \quad (\text{A4})$$

394
 395 where $B = (\partial \ln \text{CO}_2 / \partial \ln C_{sat})$ is the Revelle Buffer factor expressing how fractional chemical in
 396 atmospheric CO_2 are much larger than fractional changes in DIC with B the order 10 for the present
 397 ocean (e.g. *Williams and Follows, 2011*). Substituting (A4) into (A3), and noting that $I_{ocean} = VC_{DIC}$,
 398 produces an identity for δI_{ocean} containing a term in $\delta \ln \text{CO}_2$,

$$400 \quad \delta I_{ocean} = \frac{I_{ocean}^{sat}}{B} \delta \ln \text{CO}_2 + V \left(\delta C_{dis} + \delta C_{bio} + \frac{\partial C_{sat}}{\partial A_{pre}} \delta A_{pre} + \frac{\partial C_{sat}}{\partial T_{oc}} \delta T_{oc} \right), \quad (\text{A5})$$

401
 402 where $I_{ocean}^{sat} = VC_{sat}$ is the ocean inventory of saturated DIC at current atmospheric CO_2 .
 403 Substituting δI_{ocean} (A5) and δI_{atmos} (A1) into (7), and re-arranging to solve for the log change in
 404 atmospheric CO_2 mixing ratio to small perturbations to I_{em} , I_{ter} , C_{dis} , C_{bio} , A_{pre} and T_{oc} , reveals
 405

$$\left(I_{atmos} + \frac{I_{ocean}^{sat}}{B} \right) \delta \ln \text{CO}_2 = \delta I_{em} - \delta I_{ter} - V \left(\delta C_{dis} + \delta C_{bio} + \frac{\partial C_{sat}}{\partial A_{pre}} \delta A_{pre} + \frac{\partial C_{sat}}{\partial T_{oc}} \delta T_{oc} \right) \quad (\text{A6})$$

406
 407 The issue now is that this identity for $\delta \ln \text{CO}_2$, (A7), applies only to small infinitesimal
 408 perturbations, and we wish to solve for the change in log CO_2 for large finite perturbations. The

409 next step is therefore to integrate (A6) over large finite perturbations in I_{em} , I_{ter} , C_{dis} , C_{bio} , A_{pre} and
 410 T_{oc} .

411
 412 To integrate (A6), we note that the left-hand side contains the buffered carbon inventory, I_B
 413 (*Goodwin et al.*, 2007; 2008), defined as the atmospheric carbon inventory added to the ocean
 414 saturated-DIC inventory divided by the Revelle Buffer factor, $I_B = I_{atmos} + \left(I_{ocean}^{sat} / B \right)$. I_B represents
 415 the total buffered CO₂ and DIC in the atmosphere-ocean system that is available for redistribution
 416 between the CO₂ and carbonate ion pools (*Goodwin et al.*, 2009), given that the majority of ocean
 417 DIC is in the form of bicarbonate ions. At the preindustrial state, $I_B=3451\pm96$ PgC in the CMIP5
 418 models analyzed by *Williams et al.* (2017).

419
 420 Using this constant buffered carbon inventory approach (Supplementary), we integrate (A6) to find
 421 the change in atmospheric CO₂ for large finite perturbations to total carbon emitted, ΔI_{em} , the
 422 change in terrestrial carbon storage, ΔI_{ter} , the large changes in mean ocean values of ΔC_{dis} , ΔC_{bio} ,
 423 ΔA_{pre} and ΔT_{oc} , so that

$$424 \quad I_B \Delta \ln \text{CO}_2 = \Delta I_{em} - \Delta I_{ter} - V \left(\Delta C_{dis} + \Delta C_{bio} + \frac{\partial C_{sat}}{\partial A_{pre}} \Delta A_{pre} + \frac{\partial C_{sat}}{\partial T_{oc}} \Delta T_{oc} \right). \quad (\text{A7})$$

425
 426
 427 Multiplying (A7) by the CO₂-radiative forcing coefficient, a , produces an expression for the
 428 radiative forcing from CO₂ in (9),

$$429 \quad \Delta R_{CO_2} = \Delta R_{CO_2}^{forcing} + \Delta R_{terrestrial}^{feedback} + \Delta R_{ocean}^{feedback},$$

430
 431
 432 as a sum of separable terms representing different processes, each linked to a different change in a
 433 carbon inventory. The CO₂ radiative forcing,
 434

$$435 \quad \Delta R_{CO_2}^{forcing} = (a/I_B)(\Delta I_{em} - V\Delta C_{dis}), \quad (\text{A8a})$$

436
 437 represents the direct effect of the emitted carbon partitioned between the atmosphere and ocean,
 438 including both chemical equilibrium (ΔI_{em}) and the transient chemical disequilibrium between the
 439 atmosphere and ocean (ΔC_{dis}) of the carbon emitted, but without subsequent carbon feedbacks. The
 440 radiative forcing from the carbon feedbacks for the terrestrial,
 441

442 $\Delta R_{terrestrial}^{feedback} = -(a/I_B)\Delta I_{ter},$ (A8b)

443

444 depends on the change in terrestrial carbon storage since the preindustrial, and for the ocean

445

446 $\Delta R_{ocean}^{feedback} == -(a/I_B)V(\Delta C_{bio} + [\partial C_{sat}/\partial A_{pre}]\Delta A_{pre} + [\partial C_{sat}/\partial T_{oc}]\Delta T_{oc}),$ (A8c)

447

448 depends on the changes to the ocean biological drawdown of soft tissue and CaCO₃, including the

449 titration alkalinity effects, and from changes in the seawater temperature since the preindustrial,

450 altering the solubility of CO₂ in seawater.

451

452 **Acknowledgements:**

453 We acknowledge global surface temperature anomaly data from GISTEMP Team, 2018: GISS

454 Surface Temperature Analysis (GISTEMP). NASA Goddard Institute for Space Studies. Dataset

455 accessed 2018-01-16 at <https://data.giss.nasa.gov/gistemp/>. We acknowledge the Global Carbon

456 Project's Global Carbon Budget 2018 for the land carbon sink data, including the multi-model mean

457 from 16 DGVMs from year 1750 to 1959 and the model breakdowns from these models from years

458 1959 to 2017. We thank Stephen Sitch for providing additional data from these 16 Global Carbon

459 Project DGVMs prior to 1959, allowing the inter-model standard deviation in the inter-model

460 cumulative land carbon sink, ΔI_{ter} , to be calculated. The authors acknowledge the World Climate

461 Research Programmes Working Group on Coupled Modelling responsible for CMIP5. This work

462 was funded by UK NERC grant NE/N009789/1 and combined UK NERC/UK Government

463 Department of BEIS grant NE/P01495X/1.

464

465 **References:**

466 Archer, D. (2005) Fate of fossil fuel CO₂ in geologic time. *Journal of Geophysical Research*,

467 110 (C9), C09S05, doi:10.1029/2004JC002625.

468

469 Andrews, T., Gregory, J.M., Webb, M.J. and Taylor, K.E., (2012) Forcing, feedbacks and climate

470 sensitivity in CMIP5 coupled atmosphere-ocean climate models. *Geophysical Research*

471 *Letters*, 39(9).

472

473 Andrews, T., Gregory, J.M. and Webb, M.J. (2015) The dependence of radiative forcing and

474 feedback on evolving patterns of surface temperature change in climate models. *Journal of*

475 *Climate*, 28(4), pp.1630-1648.

476

477 Armour, K.C., Bitz, C.M. and Roe, G.H., (2013) Time-varying climate sensitivity from regional
478 feedbacks. *Journal of Climate*, 26(13), pp.4518-4534.

479

480 Arneth, A., Harrison, S.P., Zaehle, S., Tsigaridis, K., Menon, S., ... & Vesala, T. (2010) Terrestrial
481 biogeochemical feedbacks in the climate system, *Nature Geoscience* 3, 525-532.

482

483 Arora, V.K., Boer, G.J., Friedlingstein, P., Eby, M., Jones, C.D., Christian, J.R., Bonan, G., Bopp,
484 L., Brovkin, V., Cadule, P. and Hajima, T. (2013) Carbon–concentration and carbon–climate
485 feedbacks in CMIP5 Earth system models. *J. Climate*, 26(15), pp.5289-5314.

486

487 Ceppi, P. and Gregory, J.M. (2017) Relationship of tropospheric stability to climate sensitivity and
488 Earth’s observed radiation budget. *Proceedings of the National Academy of Sciences*, 114(50),
489 pp.13126-13131.

490

491 Cheng, L. et al. (2017). Improved estimates of ocean heat content from 1960 to 2015. *Sci. Adv.* 3,
492 e1601545.

493

494 Friedlingstein, P., Dufresne, J.L., Cox, P.M. and Rayner, P. (2003) How positive is the feedback
495 between climate change and the carbon cycle?. *Tellus B*, 55(2), pp.692-700.

496

497 Friedlingstein, P., Cox, P., Betts, R., Bopp, L., von Bloh, W., Brovkin, V., ... and Bala, G., (2006)
498 Climate–carbon cycle feedback analysis: results from the C4MIP model intercomparison. *J.*
499 *Climate*, 19(14), pp.3337-3353.

500

501 Frölicher, T. L. and Paynter, D.J. (2015) Extending the relationship between global warming
502 and cumulative carbon emissions to multi-millennial timescales. *Environmental Research*
503 *Letters*, 10 (7), 075 002.

504

505 Gillett, N.P., Arora, V.K., Matthews, D. and Allen, M.R., 2013. Constraining the ratio of global
506 warming to cumulative CO₂ emissions using CMIP5 simulations. *J. Climate*, 26(18), pp.6844-6858.

507

508 Goodwin, P., (2018) On the time evolution of climate sensitivity and future warming, *Earth’s*
509 *Future* 6, EFT2466, doi:10.1029/2018EF000889.

510

511 Goodwin, P., A. Katavouta, V.M. Roussenov, G.L. Foster, E.J. Rohling and R.G. Williams, (2018)
512 Pathways to 1.5 and 2 °C warming based on observational and geological constraints, *Nature*
513 *Geoscience* 11, 102-107, doi:10.1038/s41561-017-0054-8.

514

515 Goodwin, P. (2016) How historic simulation-observation discrepancy affects future warming
516 projections in a very large model ensemble, *Climate Dynamics*, CLDY-D-15-00368R2, doi:
517 10.1007/s00382-015-2960-z.

518

519 Goodwin, P., R.G. Williams and A. Ridgwell (2015), Sensitivity of climate to cumulative carbon
520 emissions due to compensation of ocean heat and carbon uptake, *Nature Geoscience* 8, 29-34.
521 doi:10.1038/ngeo2304.

522

523 Goodwin, P., K. I. C. Oliver, and T. M. Lenton (2011), Observational constraints on the causes of
524 Holocene CO₂ change, *Global Biogeochemical Cycles*, 25, GB3011, doi:10.1029/2010GB003888.

525

526 Goodwin, P., R.G. Williams, A. Ridgwell and M.J. Follows (2009), Climate sensitivity to the
527 carbon cycle modulated by past and future changes in ocean chemistry, *Nature Geoscience*, Vol. 2,
528 No. 2, p145-150, doi:10.1038/ngeo416.

529

530 Goodwin, P., M. J. Follows, R. G. Williams (2008), Analytical relationships between atmospheric
531 carbon dioxide, carbon emissions, and ocean processes, *Global Biogeochemical Cycles*, 22,
532 GB3030, doi:10.1029/2008GB003184.

533

534 Goodwin, P. and Lenton, T. (2009), Quantifying the feedback between ocean heating and CO₂
535 solubility as an equivalent carbon emission, *Geophysical Research Letters*, 36, L15609,
536 doi:10.1029/2009GL039247.

537

538 Goodwin, P., R.G. Williams, M.J. Follows, S. Dutkiewicz (2007), Ocean-atmosphere partitioning
539 of anthropogenic carbon dioxide on centennial timescales, *Global Biogeochemical Cycles*, 21,
540 GB1014, doi:10.1029/2006GB002810.

541

542 Gregory, J. M., Ingram, W. J., Palmer, M. A., Jones, G. S., Stott, P. A., Thorpe, R. B., ... Williams,
543 K. D. (2004). A new method for diagnosing radiative forcing and climate sensitivity. *Geophysical*
544 *Research Letters*, 31, L03205, doi.org/10.1029/2003GL018747
545

546 Gregory, J. M., Jones, C. D., Cadule, P. & Friedlingstein, P. (2009) Quantifying carbon cycle
547 feedbacks. *J. Clim.* 22, 5232–5250.
548

549 Hansen, J., Ruedy, R., Sato, M. and Lo, K., (2010) Global surface temperature change, *Rev.*
550 *Geophys.*, 48, RG4004, doi:10.1029/2010RG000345.
551

552 IPCC (2013) *Climate Change 2013: The Physical Science Basis* (eds Stocker, T. F. et
553 al.) (Cambridge Univ. Press, Cambridge, 2013).
554

555 Ito, T., and Follows, M.J. (2005), Preformed phosphate, soft tissue pump and atmospheric CO₂, *J.*
556 *Mar. Res.*, 63(4), 813– 839, doi:10.1357/0022240054663231.
557

558 Knutti, R., Rugenstein, M.A.A. and Hergerl, G.C. (2017) Beyond equilibrium climate sensitivity,
559 *Nature Geoscience* 10, 727-736, DOI:10.1038/ngeo3017.
560

561 le Quéré et al. (2018). Global Carbon Budget 2017, *Earth Syst. Sci. Data*, 10, 405-448, doi:
562 10.5194/essd-10-405-2018.
563

564 MacDougall, A. H. and Knutti, R. (2016). Projecting the release of carbon from permafrost
565 soils using a perturbed physics ensemble modelling approach. *Biogeosciences*, 13, 2123–
566 2136, doi: 10.5194/bg-13-2123-2016.
567

568 Meinshausen, M. et al. (2011). The RCP greenhouse gas concentrations and their extensions from
569 1765 to 2300. *Climatic Change* 109, 213–241.
570

571 Myhre, G., et al. (2013) Anthropogenic and Natural Radiative Forcing Supplementary Material. In:
572 *Climate Change 2013: The Physical Science Basis. Contribution of Working Group I to the Fifth*
573 *Assessment Report of the Intergovernmental Panel on Climate Change* [Stocker, T.F., D. Qin, G.-K.
574 Plattner, M. Tignor, S.K. Allen, J. Boschung, A. Nauels, Y. Xia, V. Bex and P.M. Midgley (eds.)].
575

576 Pugh, T. A. M., Jones, C. D., Huntingford, C., Burton, C., Arneeth, A., Brovkin, V., et al. (2018). A
577 large committed long-term sink of carbon due to vegetation dynamics. *Earth's Future*, 6.
578 <https://doi.org/10.1029/2018EF000935>.
579

580 Rohling, E. J., Marino, G., Foster, G. L., Goodwin, P. A., von der Heydt, A. S., & Köhler, P.
581 (2018). Comparing climate sensitivity, past and present. *Annual Review of Marine Science*, 10,
582 261–288. <http://www.annualreviews.org/doi/full/10.1146/annurev-marine-121916-063242>.
583

584 Schwinger, J., Tjiputra, J.F., Heinze, C., Bopp, L., Christian, J.R., Gehlen, M., Ilyina, T., Jones,
585 C.D., Salas-Méllia, D., Segschneider, J. and Séférian, R. (2014) Nonlinearity of ocean carbon cycle
586 feedbacks in CMIP5 earth system models. *Journal of Climate*, 27(11), pp.3869-3888.
587

588 Williams, R.G., Roussenov, V., Goodwin, P., Resplandy, L. and Bopp, L. (2017) Sensitivity of
589 global warming to carbon emissions: effects of heat and carbon uptake in a suite of Earth system
590 models, *Journal of Climate* 30, 9343-9363, doi:10.1175/JCLI-D-16-0468.1
591

592 Williams, R. G., P. Goodwin, A. Ridgwell, and P. L. Woodworth (2012), How warming and steric
593 sea level rise relate to cumulative carbon emissions, *Geophys. Res. Lett.*, 39, L19715,
594 doi:10.1029/2012GL052771.
595

596 Williams R.G. and Follows, M.J. (2011) *Ocean Dynamics and the Carbon Cycle: Principles and*
597 *Mechanisms*. Cambridge University Press, ISBN: 9780521843690. 416pp.
598

599

600 Williamson, D., Blaker, A.T., Hampton, C. & Salter, J. (2015). Identifying and removing structural
601 biases in climate models with history matching. *Climate Dynamics* 45, 1299-1324.
602 doi:10.1007/s00382-014-2378-z.
603

604 Zickfeld, K., et al. (2013). Long-term climate change commitment and reversibility: An EMIC
605 intercomparison. *Journal of Climate*, 26 (16).
606
607
608
609

610

611 **Figure 1: Climate and carbon feedback over time for a 1000PgC emission experiment in a**
612 **large ensemble of observation-constrained simulations.** (a) Partitioning of a 1000PgC carbon
613 emission (ΔI_{em} , black line) between the terrestrial carbon (ΔI_{ter} , light blue line and shading), the
614 ocean (ΔI_{ocean} , red arrow) and the atmospheric inventories (ΔI_{atmos} , bright blue arrow). (b) Radiative
615 forcing contributions from the CO₂ forcing from emissions without carbon feedbacks (red), plus the
616 non-CO₂ feedbacks (blue) and from the carbon feedbacks (light blue). (c) Total climate feedback,
617 $\lambda_{Climate}$ (light blue line and shading), and (d) total carbon feedback, λ_{Carbon} (light blue line and
618 shading), both showing contributions from individual feedback processes (dashed lines and arrows).
619 On all panels, lines show the ensemble median, dark shading is 66% range and light shading is the
620 95% range.

621

622

623 **Figure 2: Temperature anomaly, carbon sink and carbon feedback** from observational
624 reconstructions (black: shading is $\pm 1 \sigma$ range where shown), observation-constrained WASP
625 simulations (blue: line showing median and shading 66% range) and output from 7 CMIP5 Earth
626 system models. (a) 11-year running mean surface temperature anomaly relative to pre-1900
627 average. Observational reconstructions from GISTEMP. (b) Cumulative terrestrial carbon sink.
628 Observational reconstructions from the Global Carbon Budget (GCB) with additional output from
629 16 DGVMs to calculate uncertainty. (c) Terrestrial carbon feedback, λ_{Carbon} (eq. 11). Observational
630 reconstructions from GISTEMP and GCB from 1959 to 2017, and simulations using RCP4.5
631 scenario to project to year 2100. (d) Ocean carbon feedback, λ_{Carbon} , from the CO₂ solubility effect
632 only (dotted lines) and from both ocean biological drawdown and CO₂ solubility effects (dashed
633 lines). Observational reconstructions (black dotted line) derived from *Cheng et al. (2017)* ocean
634 heat uptake combined with GISTEMP.

635

636 **Figure 3: Observational constraints on climate feedback and climate sensitivity from both**
637 **physical and carbon cycle feedbacks.** (a) Climate feedback frequency distributions (solid lines)
638 and median value (dotted lines) for $\lambda_{Climate}$ (blue) and $\lambda_{Climate+Carbon} = \lambda_{Climate} + \lambda_{Carbon}$ (black). Orange
639 arrow shows the contribution of carbon feedback, λ_{Carbon} , to the median values. (b) Climate
640 sensitivity frequency distributions for $S_{Climate}$ (blue) and $S_{Climate+Carbon}$ (black), with orange arrow
641 showing impact of carbon feedbacks on the median. (c) Equilibrium Climate Response to carbon
642 Emission (ECRE) frequency distribution (black).

Figure 1.

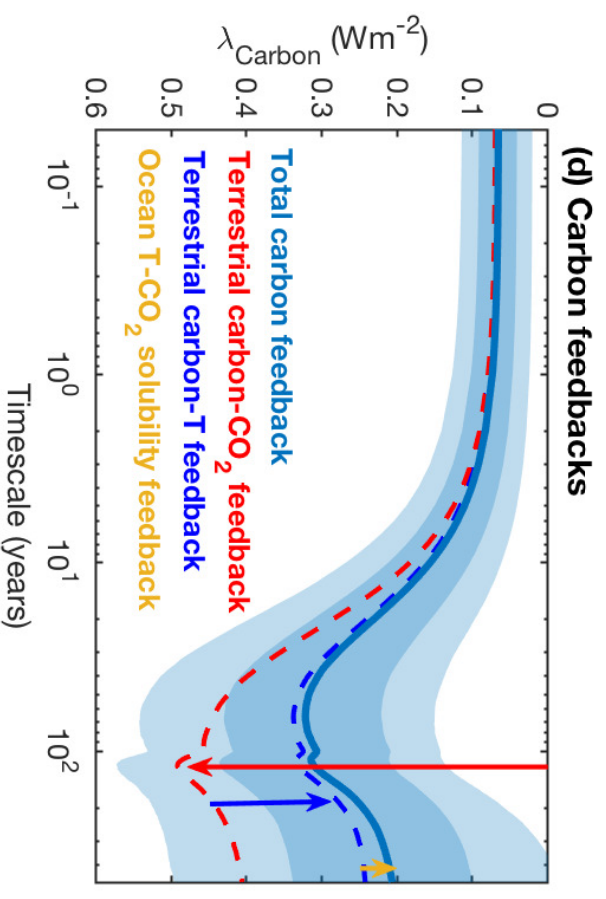
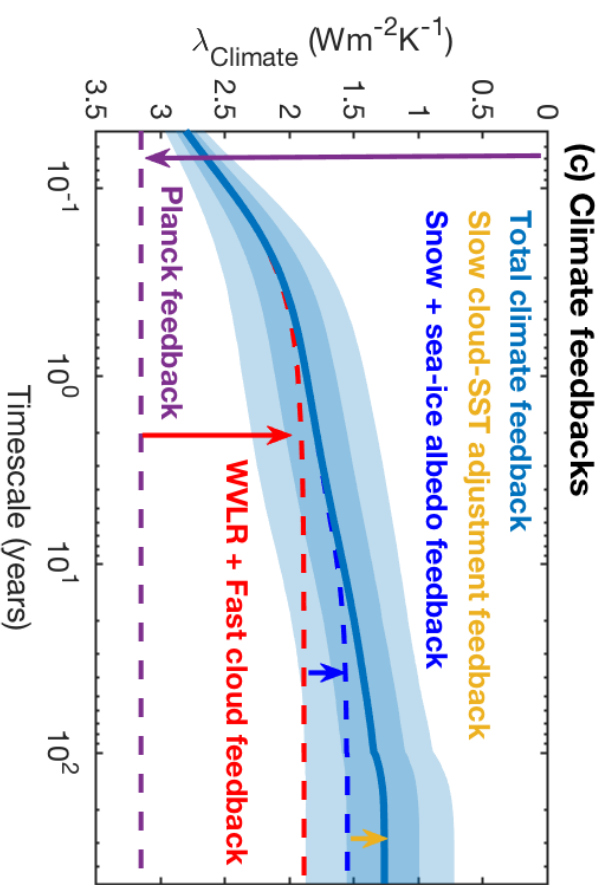
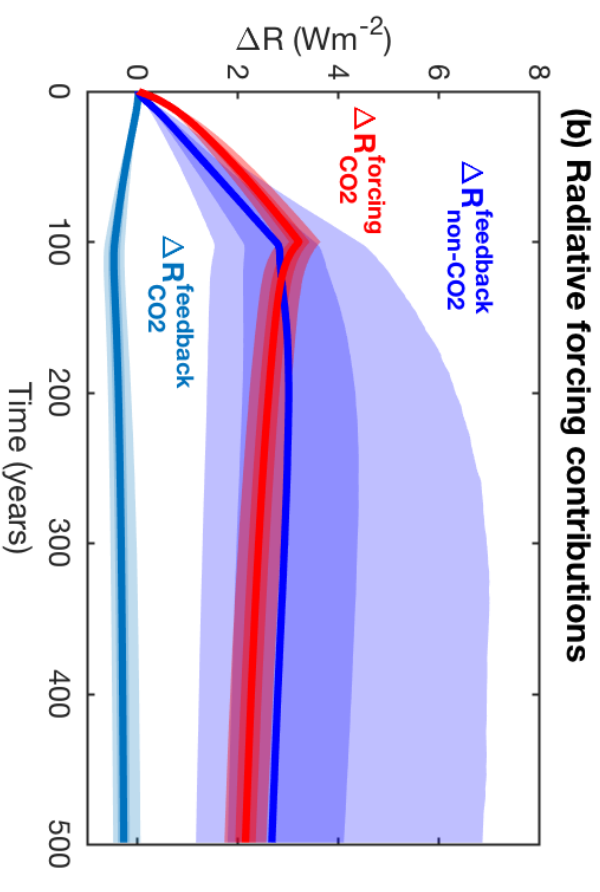
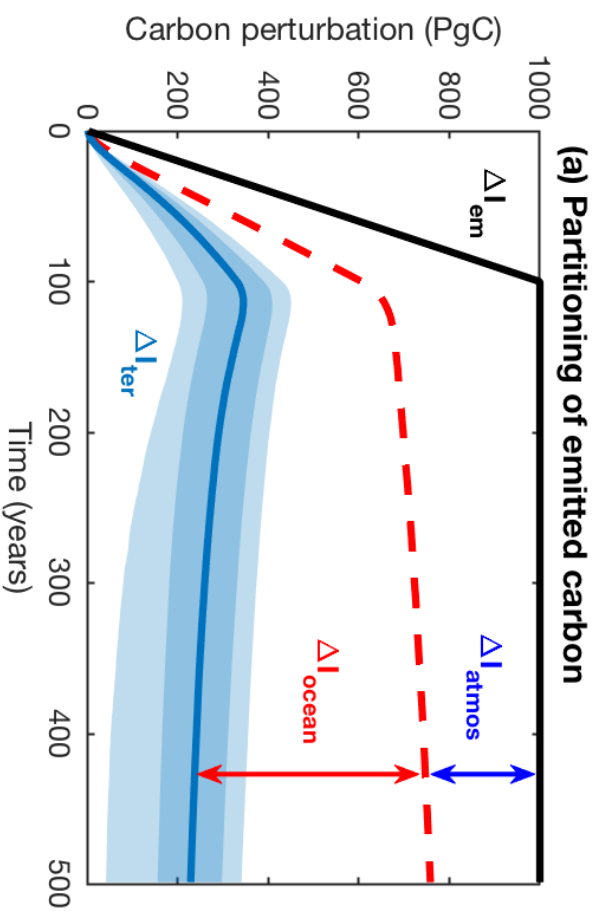


Figure 2.

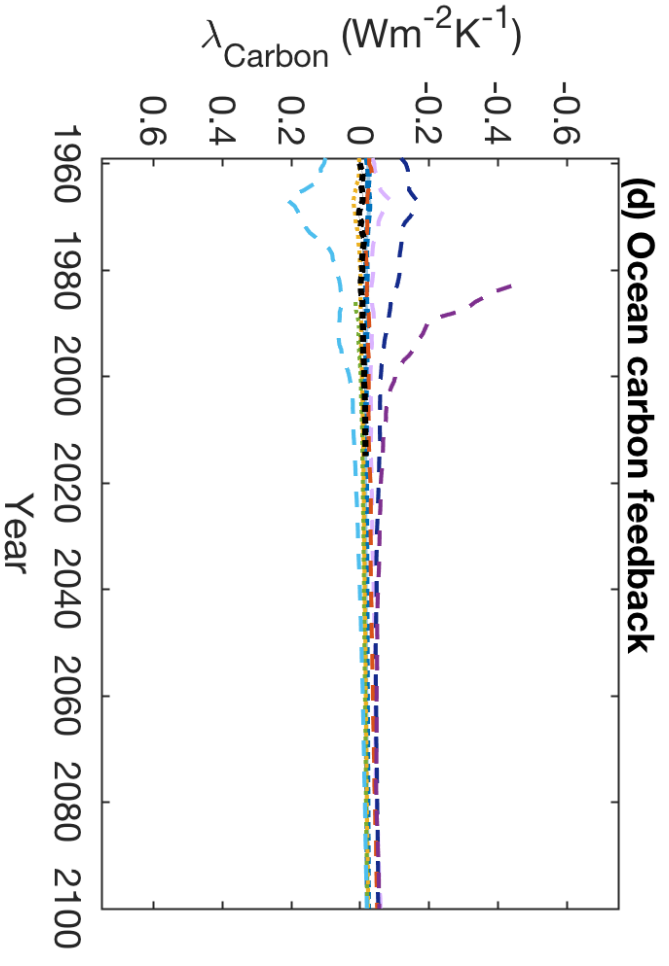
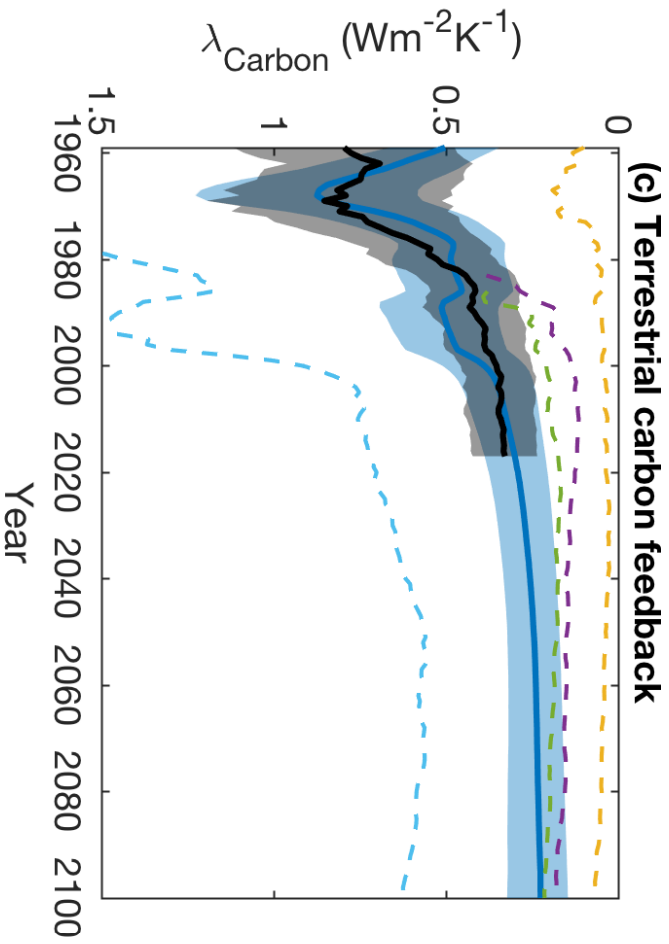
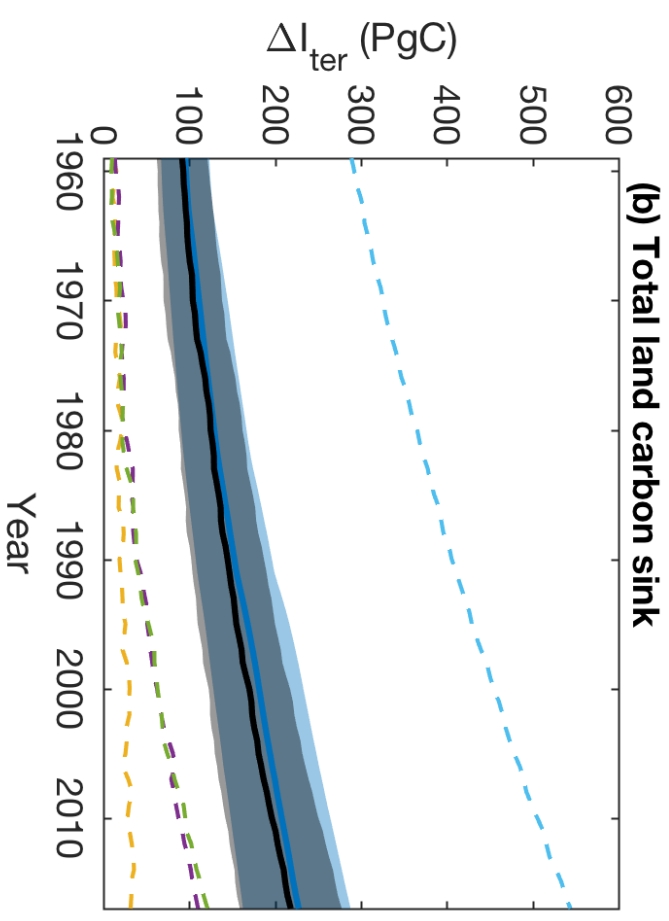
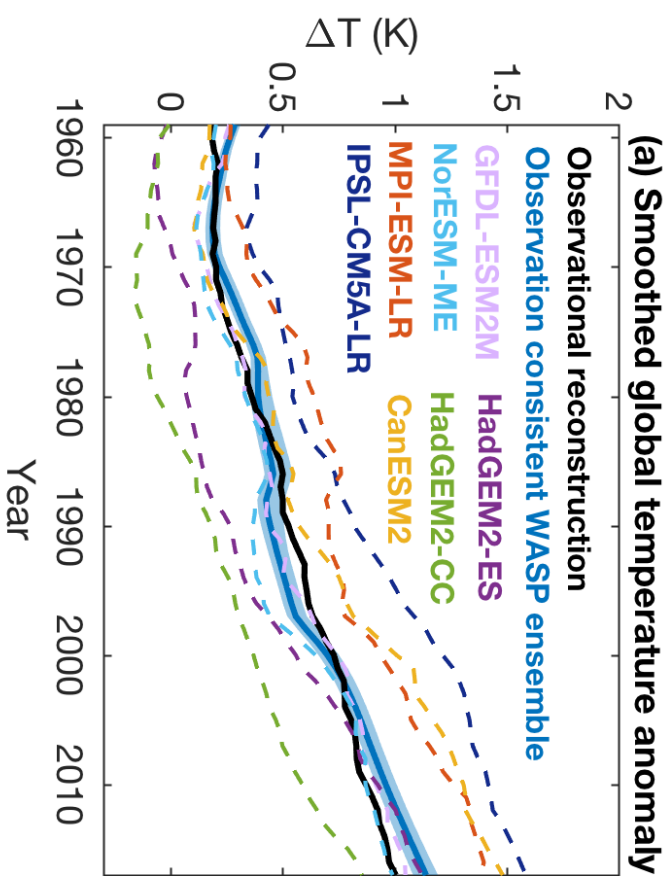
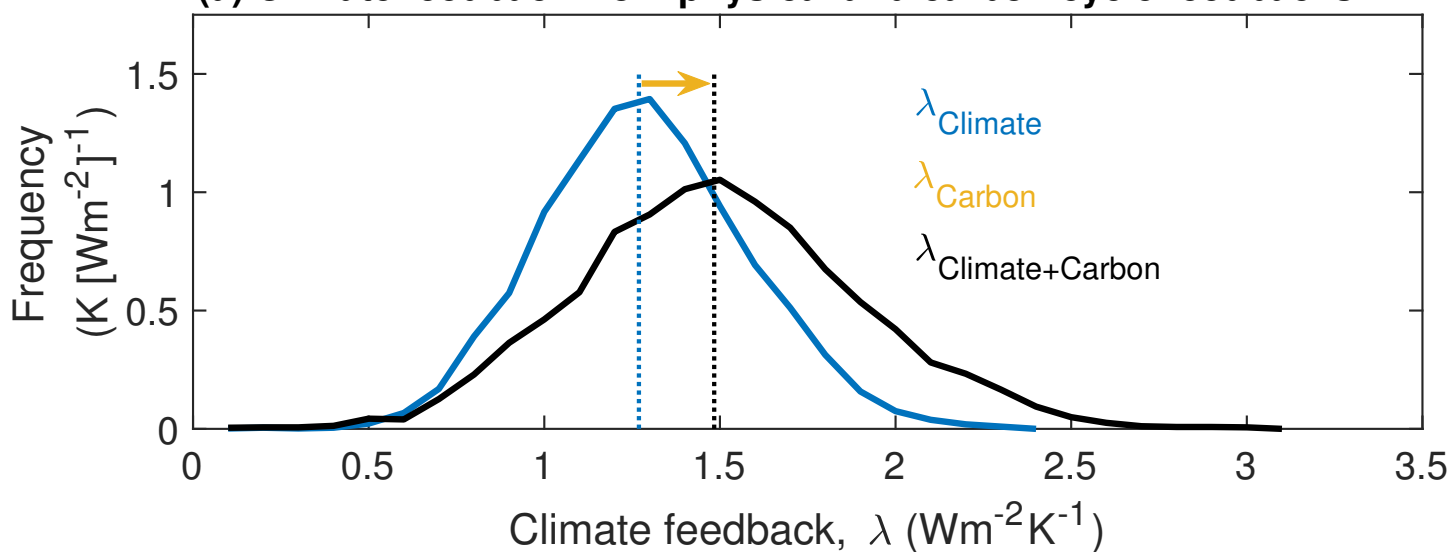
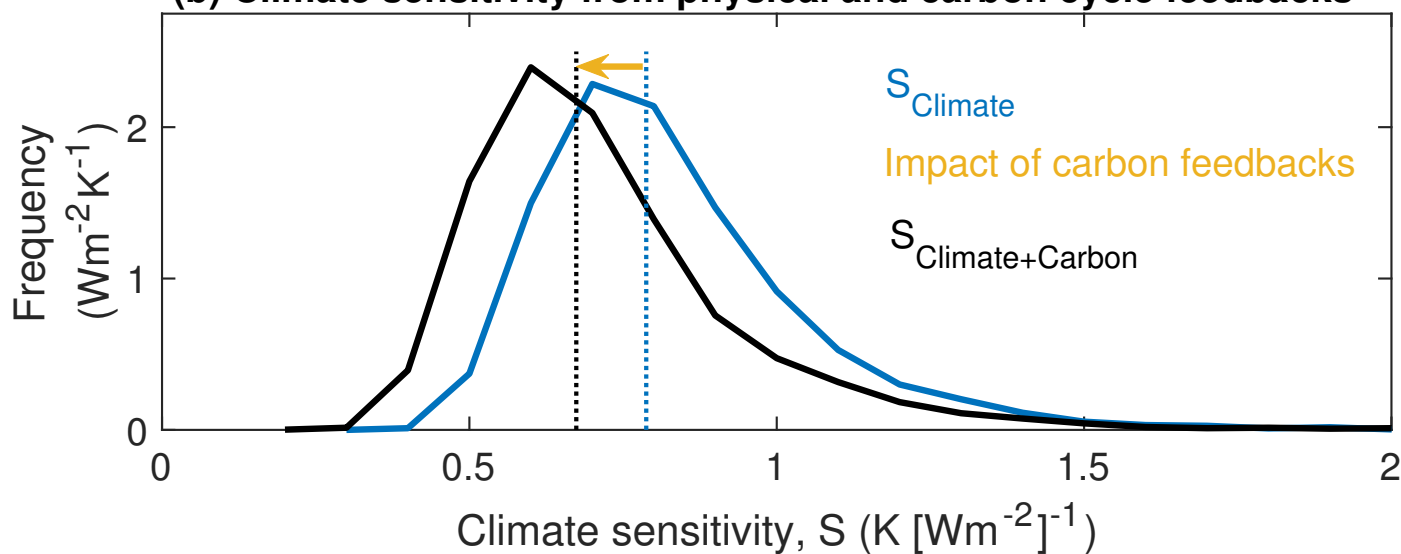


Figure 3.

(a) Climate feedback from physical and carbon cycle feedbacks



(b) Climate sensitivity from physical and carbon cycle feedbacks



(c) Equilibrium Climate Response to carbon Emission

